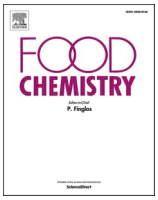
Food Chemistry 457 (2024) 140132



Contents lists available at ScienceDirect

Food Chemistry

journal homepage: www.elsevier.com/locate/foodchem





Clarification of red grape juice by amine-functionalized magnesium silica aerogel

Ilkay Turhan Kara [a,b,*], Sevil Yücel [b], Muhammet Arici [c]

[a] Department of Nutrition and Dietetics, School of Health Sciences, Istanbul Arel University, Zeytinburnu 34010, Istanbul, Turkey
[b] Department of Bioengineering, Faculty of Chemistry and Metallurgy, Yildiz Technical University, Esenler, 34210 Istanbul, Turkey
[c] Department of Food Engineering, Faculty of Chemistry and Metallurgy, Yildiz Technical University, Esenler, 34210 Istanbul, Turkey

ARTICLE INFO

Keywords:
Red grape juice
Clarification
APTES
Magnesium silica aerogel
Box-Behnken
Electrostatic interaction
Color components

ABSTRACT

The clarification conditions and the selection of the clarification agent are pivotal in eliminating the haze components from red grape juice (RGJ) while minimizing the loss of functional color components. In this context, we synthesized a water glass-based APTES functionalized magnesium silica aerogel (MSA-NH_3) incorporating 61.44 molecules/nm^2 of amine groups, resulting in a positively charged zeta potential value of 33.9 mV (pH 3.4) for clarification of RGJ by targeting negatively charged polyphenols. The optimum clarification conditions using MSA-NH_3 were determined as 0.18 g MSA-NH_3/L RGJ, 20 °C, and 60 min through the application of Box-Behnken design. Under these conditions, MSA-NH_3 exhibited excellent adsorption of haze components (3.61 NTU), outperforming the commercial bentonite-gelatine combination (BGC) (5.45 NTU). Furthermore, it exhibited greater efficacy in preserving anthocyanins while adsorbing browning components. MSA-NH_3 has a high potential to serve as a functional alternative clarification agent in the beverage industry due to its promising clarification performance.

1. Introduction

Grapes and grape-derived products are widely produced and consumed worldwide, partly because of their associated health benefits depending on possessing high amounts of bioactive compounds, especially polyphenols (Zhou et al., 2022). Pressed fruit juices have a cloudy appearance because of (Kandylis, 2021) their naturally existing compounds (Arslan Kulcan et al., 2015) and the most frequent cause of haze in clear beverages like fruit juices, results from haze active (HA) protein - haze active (HA) polyphenol (Siebert, 1999). Grape juices have low HA protein content but are much more variable in terms of HA polyphenol content (Siebert, 1999; Siebert et al., 1996). Most consumers prefer clear juice because they perceive it as more palatable and fresher than cloudy juices. In this regard, to produce a clear RGJ, the removal of both proteins and phenolics should be targeted (Dıblan & Özkan, 2021).

The utilization of fining agents such as bentonite gelatine and silica sol is one of the conventional clarification methods in the fruit juice industry (Hatamikia et al., 2013). Bentonite is a type of clay from the montmorillonite group, and its negatively charged surfaces adsorb electrostatically positively charged proteins and anthocyanins (ACNs). As a consequence of adsorbing the ACNs at high dosages, bentonite reduces the bright red color of RGJ and red wine (Dıblan & Özkan, 2021; Stankovic et al., 2012). Protein-based clarifying agents especially gelatin can be used for the effective removal of high molecular weight (>500 Da) polyphenols due to their positive charges at the acidic juice pHs, including RGJ with a pH of 3.3–3.9 (Dıblan & Özkan, 2021). However, during clarification, the interaction between gelatin and phenolics and/or bentonite leads to flocculation, causing ACNs to be removed along with these flocks. As a result, gelatin indirectly reduces the bright red color of beverages. For effective clarification in anthocyanin-rich fruit juices, low turbidity together with high anthocyanin retention are considered as the major indicators (Orhan Dereli et al., 2023). Furthermore, excessive use of gelatin, a protein-based clarifying agent, can result in turbidity during storage (Turfan, Türkyilmaz, Yemi, & Özkan, 2011). It can also lead to raising concerns among consumers due to cultural and health risks (Mariod & Fadul, 2013; Zhang et al., 2017),

Abbreviations: MSA, magnesium silica aerogel; MSA-NH_3, amine-functionalized magnesium silica aerogel; ACN, Anthocyanin; BGC, Bentonite Gelatin Combination; NTU, Nephelometric Turbidity Units; PC %, Percent Polymeric Color; RGJ, Red Grape Juice; TPC, Total Phenolic Content; RSM, Response Surface Methodology.

* Corresponding author at: Department of Nutrition and Dietetics, School of Health Sciences, Istanbul Arel University, Zeytinburnu, 34010 Istanbul, Turkey.
E-mail address: ilkayturhan@arel.edu.tr (I. Turhan Kara).

https://doi.org/10.1016/j.foodchem.2024.140132
Received 12 March 2024; Received in revised form 1 June 2024; Accepted 14 June 2024
Available online 19 June 2024
0308-8146/© 2024 Elsevier Ltd. All rights are reserved, including those for text and data mining, AI training, and similar technologies.

and is not preferred due to sustainability or animal cruelty issues, particularly by vegan consumers (Ramezani et al., 2020). Although researchers have developed fining agents to replace animal proteins, such as gluten, legume, potato, maize, and yeast protein extracts, due to concerns about the use of animal-derived proteins in the food sector, the general allergy potential of proteins, regardless of their plant or animal origin, has posed a different concern (Kemp et al., 2021). Additionally, the combined use of gelatin and bentonite is quite common for dark-coloured beverages industrially. However, this practice not only eliminates their potential for reuse but also can pose environmental risks for the disposal of a mixture of materials with different origins. The diverse concerns linked to existing fining agents have prompted the exploration of alternative methods, propelling promising advancements in nanotechnology (Kemp et al., 2021).

Synthetic magnesium silicates are widely utilized in the food industry because of their superior adsorption properties for undesirable components, and their surface properties can be enhanced through chemical synthesis methods on a nanoscale (Ghods et al., 2016; Lu et al., 2016). Silica aerogels are a unique class of silica-based mesoporous materials; and they have been the matter of intense academic research with their 3D network structure, high porosity (>80%) and surface area (>500 m^2/g) result in exceptional performance as adsorbents for organic pollutants (Gurav et al., 2010; Maximiano et al., 2019) such as pharmaceutical compounds (Mohseni-Bandpei et al., 2020), free fatty acids, peroxide value, phosphorus, and color pigments (Soylu et al., 2024), heavy metals (Ghahremani et al., 2021; Ihsanullah et al., 2022), pesticides (Lin et al., 2024), cationic and anionic dyes (Chen et al., 2021), phenol (Qin et al., 2013). The adsorption mechanism of organic materials by the silica aerogel involves hydrogen bonding, hydrophobic, diffusion into the internal pores, and electrostatic interactions (Mohseni-Bandpei et al., 2020). Pure silica samples display negative values of zeta potential due to silanol groups onto the surface of the particles (Barczak, 2019) and silica aerogel with an isoelectric point below 3.5 is suitable for attracting electron-deficient species, such as cationic compounds (Mohseni-Bandpei et al., 2020; Parida et al., 2006; Ulker & Erkey, 2014).

One of the most important properties of silica-based nanoparticles is their ability to be modified with a wide variety of functional groups such as amino groups which increases the selectivity, effectiveness, capacity, and stability of the inorganic silica adsorbent in the organic solvent (Hozhabr Araghi & Entezari, 2015). Incorporation of amine groups results in a significant change in the surface charges. At low pH values, the protonated amino groups cause the zeta potential value to shift from negative to highly positive values, indicating the presence of a positively charged surface on amine-functionalized silica. Thus, electrostatic interactions occur between the amine-modified silica surface and negatively charged anions (Barczak, 2019) such as phenolic compounds in fruit juice acidic condition. Organo-silanes can be utilized to improve the physical, chemical, and mechanical properties of food contact materials in a wide variety of applications in the food and beverage industry (Kregiel, 2014). 3-aminopropyltriethoxysilane (APTES) can be used as a polymer coating material, according to a 2005 EFSA (European Food Safety Authority) report The European Food Safety Authority (EFSA), (2005).

Due to their adjustable pore size, high thermal stability, distinct adsorption properties, unique 3D structures, several mesoporous nanomaterials have been effectively utilized to prevent protein haze in wines, with less aroma loss compared to Na bentonite treatment. Zirconium dioxide/Zirconia (ZrO2), a metal oxide, has shown potential in removing haze-forming proteins in continuous and batch-wise applications, both during and after fermentation (Van Sluyter et al., 2015). Acrylic acid plasma polymer coated magnetic nanoparticles (MNP) were immersed in unstable wines, then removed with magnets along with specifically the haze-forming proteins but phenolic compounds were unaffected (Mierczynska-Vasilev et al., 2017). The materials also have remarkable properties, such as being regenerable and reusable, which are important for sustainability (Kemp et al., 2021; Van Sluyter et al., 2015). These results highlight that mesoporous nanomaterials and nanoparticles shows promise in clear beverage production. Although there are various studies in the literature where silica gel and APTES were used together or separately in fruit juice clarification, these materials were generally employed not for direct clarification purposes, but indirectly as carrier materials for the clarification agents such as enzymes (Mohammadi et al., 2020; Muley et al., 2018; Ozyilmaz & Gunay, 2023; Sojitra et al., 2016). However, not much attention has been given to the study of using silica aerogel-based materials for the clarification of beverages, despite the limitations of traditional clarification adsorbents. Studies on current mesoporous materials focus on clarifying light-colored beverages as an alternative to clays like bentonite for protein haze removal, as discussed above (Kemp et al., 2021; Mierczynska-Vasilev et al., 2017; Van Sluyter et al., 2015). However, there is a need for adsorbents that can selectively remove phenolic compounds causing turbidity, especially in clear dark-coloured beverages, reducing reliance on animal-based protein adsorbents and addressing sustainability concerns. To the best of the authors' knowledge, the use of silica aerogel-based materials for RGJ clarification and the effects of clarification conditions with MSA-NH_3 on haze and color components, along with their optimization, have not been previously reported. This study is the first to examine the clarification potential of aerogels for the clear red grape juice industry.

The outcome of clarification processes is greatly influenced by various working conditions, including the quantity of clarification agents, time, temperature, pH, and so on. Therefore, optimizing the working conditions of these new adsorbents is crucial to achieving the most efficient results. Response Surface Methodology (RSM), which is less labor-intensive and time-consuming, reveals the individual and interactive effects of factors on responses by applying a combination of statistical and mathematical techniques. It has been widely implemented and used for improving and optimizing clarification processes in the food industry (Lee et al., 2006; Liew Abdullah et al., 2007; Ozyilmaz & Gunay, 2023; Tastan & Baysal, 2015).

The objective of this study is to determine the optimal clarification conditions for RGJ using MSA-NH_3 through RSM and compare its selective adsorption potential with commercial single-use fining agents, which include animal-derived agents. For this purpose, MSA, previously synthesized under optimal conditions (Kara et al., 2020), was functionalized with APTES to introduce positive charges, enhance its adsorption properties, and then characterized. Various parameters such as time, temperature, and concentration of MSA-NH_3 were optimized using RSM-Box-Behnken. The effects of MSA-NH_3 treatment on turbidity, ACN content, total phenolic content (TPC), and color components of RGJ were assessed. Lastly, the clarification performance of MSA-NH_3 was compared with a widely used industrial clarification agent, a bentonite-gelatine combination (BGC).

2. Materials and methods

2.1. Grapes and grape juice

RGJ was obtained from grapes (*Vitis vinifera L.,* cv. Hamburg muscat) grown in the vineyards of Tekirdağ Viticulture Research Institute (Republic of Turkey Ministry of Agriculture and Forestry) in Tekirdağ, Turkey. The harvest of grapes to be processed into RGJ was carried out when the maturity index (water-soluble dry matter/acid) values between 20 and 30, which were reported as the most suitable value for grape juices (Canbaş et al., 1996) were reached. Harvested grapes were washed with drinking tap water from dust and impurities, and rotten and raw parts that could not be processed were removed. After the grapes separated from their stems were crushed, obtained mashes were heated at 40–50 °C for 1 h and the RGJ was taken by pressing. Grape must (turbid raw grape juice) was pasteurized in 3 L jars at 85C for 15 s. Pasteurized RGJ was stored at room conditions until used in the experiments.

2.2. Chemicals and reagents

Magnesium chloride hexahydrate ($MgCl_2.6H_2O$), ethanol (absolute), tetraethyl orthosilicate (TEOS), n-heptane, toluene, sodium hydroxide (NaOH), sodium carbonate (Na_2CO_3), sodium chloride (NaCl), hydrochloric acid (HCl), Folin-Cioacalteus reagent, phenolphthalein were purchased from Merck Co. (Darmstadt, Germany). 3-aminopropyltriethoxysilane (APTES), potassium metabisulfite ($K_2S_2O_5$), gallic acid, potassium chloride (KCl), sodium acetate (NaOAc) were purchased from Sigma-Aldrich Co. (St. Louis, MO, U.S.A.). Water glass ($Na_2O{:}3.2SiO_2$) was purchased from Ege Kimya Co. (İstanbul, Turkey). Bentonite was purchased from Clariant International Ltd. (Muttenz Switzerland) and gelatin (A type, 80 Bloom strength) Pektinex® Ultra Clear from Novozymes Co. (Bagsvaerd, Denmark). All reagents were analytical grade.

2.3. Synthesis of MSA-NH_3

MSA was traditionally synthesized via the sol-gel method consisting of 3 steps (gel-like structure formation, aging-solvent exchange, and drying). The detailed preparation process, optimization, and characterization of water glass-based MSA were described in our previous study (Kara et al., 2020). After MSA synthesis, the surface of the MSA was functionalized using APTES by the post-grafting method where chemical groups were introduced to the surface of synthesized aerogels (Howarter & Youngblood, 2006). For surface functionalization, 2 g of MSA powder was ultrasonically dispersed in toluene/APTES (92.5:7.5 *v/v*) mixture. The ratio of the toluene/APTES mixture was determined after preliminary studies. Toluene, APTES, and silica aerogel mixture were stirred under reflux at 75 °C for 24 h with a magnetic stirrer. After 24 h, the mixture was allowed to cool to room temperature, and functionalized MSA was washed three times with toluene to remove unbound silane. MSA-NH_3 was dried at 80 °C in a vacuum dryer (Binder, Germany).

2.4. Characterization of MSA-NH_3

MSA and MSA-HN_3 were characterized by several techniques. Specific surface area, pore size, and pore volume analysis of MSA and MSA-NH_3 were performed with the Automatic Surface Area and Pore Size Distribution Analyzer (Micrometrics, TriStar II 3020). Nitrogen gas (N_2) adsorption–desorption isotherms were measured at 77 K. Dried samples were degassed under nitrogen gas flow at 90 °C for 1 h and 250 °C for 2 h before the nitrogen gas adsorption/desorption measurements. The specific surface area values of the aerogels were estimated by the Brunauer-Emmett-Teller (BET) method. Pore size and pore volumes of the samples were calculated by the Barrett–Joyner–Halenda (BJH) method. The chemical structures of the aerogels were determined by The Fourier-Transform Infrared Spectroscopy (FT-IR) (Shimadzu IR Prestige 21, Kyoto, Japan) in 4000–650 cm^{-1} wavenumber range. Morphologies of MSA and MSA-NH_3 were displayed by Scanning Electron Microscopy (SEM) (Zeiss EVO® LS 10 T) with 5 kV at different magnifications and the elemental components of the aerogels were determined with Energy Dispersive Spectroscopy (EDS) (EDAX- Element EDS, AMETEK, INC., PA 19312, ABD). The Zeta potential of MSA and MSA-NH_3 were measured by using Zetasizer (Nano ZS, Malvern Instruments, England). For the zeta potential measurements, phosphate-buffered saline (PBS) mediums with pH 3.4 were used to evaluate the zeta potential variations of particles in acidic conditions (as in grape juice). The number of amine groups present on the MSA surface was determined with acid-base back titration experiments (Jung et al., 2012). Bulk density of the samples was calculated directly according to their mass-to-*v*olume ratio through the tapping method. The true (skeletal) density was measured through a He-pycnometer. The porosity of the samples was calculated from the following equation (Patel et al., 2009):

$$\text{Porosity}\ (\%) = \left(1 - \frac{q}{qs}\right) x\ 100 \quad (1)$$

where, qs and q are the true density and bulk density of the samples, respectively.

2.5. Clarification experiment

The RGJ fining process consisted of two stages: depectinization and clarification. Before clarification, the RGJ was filtered through a coarse filter. Then, Pectinex Ultracolor (Novozymes, Dittingen, Switzerland) color enzyme, was added to the juice and brought to a temperature of 50 °C at the dosage recommended by the manufacturer (10 g/hL), and the temperature was kept homogeneous by continuous mixing for 1 h. After this depectinization process, clarification with fining agents was applied (Özkan, 2014).

MSA-NH_3 was directly mixed with the depectinized RGJ samples without any pretreatment, following the clarification conditions determined in the Box-Behnken experimental design as described in Tables S1 and S2. The process conditions, including clarification temperature and clarification time, as well as concentrations of MSA-NH_3, were determined through preliminary trials. The preparation procedures and applied concentrations of commercial bentonite and gelatine were determined based on preliminary trials and relevant literature (Dıblan & Özkan, 2021; Ferreira et al., 2001), considering the recommendations of the grape juice supplier company. Accordingly, initially, a 0.6 g bentonite /L RGJ solution (10%, *w/v*) was added to the depectinized grape juice and stirred for 5 min. Subsequently, a 0.07 g gelatin/L RGJ solution (1%, w/v) was added, and the mixture was stand for 20 °C and 60 min, similar to the optimum clarification conditions of MSA-NH_3.

Various amounts of fining agents were added into 50 mL depectinized RGJ samples and mixed in a benchtop incubator shaker (Sartorius CERTOMAT IS, Goettingen, Germany) at various temperature and time conditions. Afterwards, The RGJ samples were kept in the refrigerator (8 °C) for 24 h and they were centrifuged at 4000 rpm for 10 min to remove the precipitated haze components with fining agents. Depectinized RGJ without any fining agent was taken as control. Subsequently, juice analyses were performed.

Clarification studies were carried out in two stages. In the first stage, clarification process conditions of RGJ using MSA-NH_3 were optimized by RSM as shown in Tables S1 and S2. In the second stage, the clarification performance of the MSA-NH_3 and BGC at operating conditions were compared in terms of the physical and chemical analyses applied to the fruit juices at the similar maximum clarity level provided by each adsorbent.

2.6. Grape juice analysis

2.6.1. Compositional Analysis

The turbidity of RGJs was measured with a turbidimeter (WTW TURB 355 IR, Germany) and expressed in nephelometric turbidity units (NTU). pH of RGJ samples was measured potentiometrically with a pH meter (Hanna Instruments HI83141 Germany). Total titratable acidity was measured according to the potentiometric titration of the acidity of the juice samples. The results were expressed as g/L with reference to anhydrous tartaric acid (Cemeroğlu, 2004).

2.6.2. Total Phenolic Content

TPC of the juice samples was quantified by the Folin–Cioacalteu method (Waterhouse, 2002). 40 μL juice was added to 3.16 mL distilled water. Folin-Ciocalteu reagent (200 μL) was added to this mixture that was held at room temperature for 1–2 min. Finally, 600 μL saturated Na_2CO_3 solution was added to this mixture. After the tubes were allowed to stand at room temperature for 120 min, the absorbances were measured at 765 nm on a UV–vis spectrophotometer (Scinco S-3100,

South Korea) with 1 cm path-length disposable cuvettes (Brand Gmbh). TPCs in juice samples were calculated from a standard curve of gallic acid ($R^2 = 0.996$) and the results were expressed as milligrams of gallic acid equivalents per L RGJ (mg/L).

2.6.3. Total Monomeric ACN Content

Total monomeric ACN content was estimated through a pH differential method (Giusti & Wrolstad, 2001). The pH of juice samples was brought to 1.0 with potassium chloride and 4.5 with sodium acetate buffers. Prior to absorbance measurements, the solutions were filtered through a 0.45 μm PVDF (polyvinylidene fluoride) filter (Millipore, Bedford, MA) to remove the haze. The absorbance of equilibrated solutions was measured at 520 nm (λ_{max}) for ACN content and 700 nm for haze correction on a UV–vis spectrophotometer (Scinco S-3100, South Korea) with 1 cm path-length disposable cuvettes (Brand Gmbh). Absorbance measurements were carried out at room temperature and made against distilled water as a blank. Pigment content was calculated as malvidin-3-glucoside (mv-3-glu) equivalents with a molecular weight of 493.5 and extinction coefficient of 28,000 L cm^{-1} mol^{-1}. The difference in absorbance values at pH 1.0 and 4.5 was directly proportional to ACN concentration. The results were expressed as milligrams of malvidin-3-glucoside equivalents per Liter RGJ (mg/L).

2.6.4. Color Measurement

The chrominance value (***L*, a* and b****) of the RGJ samples were measured at room temperature by using the Minolta Chroma meter CM-5 (Minolta Co., Ltd., Chuo-Ku, Osaka, Japan) with CIE D65 standard light source, where ***L**** is the brightness, ***a**** is the redness, ***b**** is the yellowness.

2.6.5. Percent Polymeric Color (PC %)

PC % was determined according to the bisulphite bleaching method described by Giusti & Wrolstad, 2001. The absorbance of bisulphite treated, and untreated samples were measured at 420 nm for brown pigments, 520 nm (λ_{max}) for monomeric ACNs and 700 nm for haze correction on a UV–vis spectrophotometer (Scinco S-3100, South Korea) with 1 cm path-length disposable cuvettes (Brand Gmbh). Color density was determined by summing the absorbance of the untreated sample with bisulphite at 420 and 520 nm, while polymeric color was determined as the sum of the absorbance of bisulphite treated sample at 420 and 520 nm. Absorbance measurements were carried out at room temperature and made against distilled water as a blank. The percentage of polymeric color (PC %) was calculated using the following equation:

$$PC\% = (\text{polymeric color}/\text{color density}) \times 100$$

2.7. Box–Behnken experimental design of RGJ clarification by using MSA-NH_3 and statistical analysis

Experimental design and statistical analysis were performed with RSM. Software Design-expert (version 7.0.0, Stat-Ease Inc., Minneapolis, USA) was used for design and data analysis of RSM. The three levels (1,0,−1), three factorial Box–Behnken experimental design (BBD) containing three replicates at the center point was used to find out the optimum clarification conditions of RGJ with MSA-NH_3 as a clarification agent. A total of 15 combinations were chosen randomly according to a BBD configuration for the three levels (1, 0, −1) of the three factors namely Concentration of MSA-NH_3 (A, g MSA-NH_3/L RGJ), Clarification Temperature (B, °C), Clarification Time (C, min), as shown in Table S1. Turbidity (Y1), total acidity (Y2), pH (Y3), total monomeric ACN content (Y4), TPC (Y5), (PC %) (Y6), ***L**** value (Y7), ***a**** value (Y8) and ***b**** value (Y9) were chosen as response functions. These dependent values were related to the factors by second-degree polynomial equations (Eq. 3.1–3.9). Analysis of variance (ANOVA) determined the effect of interaction between all the design factors on each response. Model terms were chosen when *p-value* (*probability*) was with a 95% confidence limit. The coefficients of the polynomial were designated as A, B, and C (linear effects), A^2, B^2, and C^2 (quadratic effects), AB, BC, AC (interaction effect). The analysis of variance (ANOVA) tables were generated and regression coefficients of individual linear, quadratic, and interaction terms were determined.

The statistical analysis was performed using IBM SPSS 27.0 software (Chicago, IL, USA) by one-way analysis of variance (ANOVA), followed by Tukey and Games-Howell post-hoc tests for multiple comparisons of grape juice analysis. All data are presented as mean ± standard deviation (S.D.) of three replicates. A p-value <0.05 was considered statistically significant. Graphs for the characterization of MSA-NH_3 were created using OriginPro 2018 software (Hampton, MA, USA).

3. Results and discussion

3.1. Synthesis and characterization of MSA-NH_3

MSA was traditionally synthesized via the sol-gel method consisting of 3 steps (gel-like structure formation, aging-solvent exchange, and drying). Sodium silicate and magnesium sources were diluted with water and a precipitated gel-like structure occurred as a result of hydrolysis and condensation reactions, respectively as we described in our previous study (Kara et al., 2020). Magnesium silicate surface includes hydrophobic parts such as siloxane (≡Si − O − Si≡) groups, as well as hydrophilic parts like isolated hydroxyl groups (−Mg − OH), individual silanol groups (≡Si − OH), and hydrogen bonds (Ciesielczyk et al., 2004). At the polycondensation step, a three-dimensional silica network structure was obtained through the formation of siloxane bridges (≡Si–O–Si≡) between the oligomers in the sol, resulting from cross-linking among the silicon atoms present in the initiating agents. Subsequently, the solvent exchange was carried out by aging and washing steps involving ethanol, TEOS/ethanol, and n-hexane, respectively. While aging in ethanol and TEOS/ethanol improved the mechanical strength and stiffness of the gel-like structure, replacing the TEOS/alcohol solution with n-heptane prohibited crack formation during the drying of the gel. The low surface tension of n-heptane led to reduce capillary stresses and the associated drying shrinkage of the gel (Nayak & Bera, 2009; Soleimani Dorcheh & Abbasi, 2008).

After MSA synthesis, the surface of MSA was functionalized through a post-grafting method using APTES molecules in toluene. Performing the functionalization reaction in a non-aqueous phase like toluene can prevent hydrolysis of alkoxy groups, hydrogen bonding of hydrolyzed alkoxy groups, and further cross-polymerization which is helpful to form a monolayer grafting. Thus, chemical interactions of the APTES molecules with the silica surface silanols result in a direct condensation of unhydrolyzed alkoxy groups with silanols, forming stable siloxane bonds. Then surface-saturated layers (dense and full coverage) are formed in a reproducible manner (Ek et al., 2003).

3.1.1. N_2 adsorption–desorption analysis

MSA produced under optimized production conditions exhibited a high surface area (734.43 m^2/g), a high pore volume (0.41 cm^3/g), and a mesoporous pore size (4.91 nm) (Kara et al., 2020). Table 1 and Fig. 1A summarized the specific surface area, pore size, pore volume, the N_2 adsorption-desorption isotherms, and the pore size distributions of MSA before and after functionalization with APTES (MSA-NH_3), respectively. These results indicated that the successful execution of functionalization. Subsequent to functionalization, the surface area and pore volume values of MSA-NH_3 exhibited a reduction, while the pore size increased. The attachment of the propyl groups, which are relatively higher molecule weight than that of hydroxy groups, onto the MSA surface resulted in a decrease in the surface area. On the contrary, a higher repelling force of the neighboring propyl group compared to hydroxyl groups led to an increase in the pore size value of MSA-NH_3 (Huang et al., 2016). Additionally, the reduction in pore volume was likely associated with the incorporation of long functional groups into the

Table 1
Properties of MSA and MSA-NH_3.

	BET Surface Area (m^2/g)	BJH pore volume (cm^3/g)	BJH pore size (nm)	Amount of amine groups (molecule/nm^2)	Zeta Potential (mV at pH 3.4)	Tap Density (g/cm^3)	True Density (g/cm^3)	Porosity (%)
MSA	734.43	0.41	4.91	–	−5.11 ± 0.54	0.12 ± 0.01	2.40 ± 0.02	95
MSA-NH_3	9.7850	0.007130	6.29	61.44 ± 0.05	33.9 ± 0.61	0.23 ± 0.02	3.12 ± 0.02	92

pores, as stated in previous studies (Tiryaki et al., 2020). The tapping density and true density of MSA-NH_3 increased from 0.12 to 0.23 g/cm^3 and from 2.40 to 3.12 g/cm^3, respectively. Moreover, it exhibited a highly porous structure (92%). Similarly, Alnaief and Smirnova (2010), produced functionalized silica aerogels with smaller surface area, higher density, larger pore radius, and smaller pore volume by liquid functionalization method. The functional groups must be located on the surface of the SiO_2 primary particles and offer good accessibility for further reactions. This can be proved by the values of C-constant obtained from the BET measurement, which indicate the polarity of the surface (Alnaief & Smirnova, 2010). The C-constant values of aerogels in our study increased from 173 to 400 after amin-functionalization. Alnaief and Smirnova (2010), explained this as a result of the presence of active accessible NH_2 groups on the aerogel surface. The amount of amine groups attached to the aerogel surface was calculated as 61.44 ± 0.05 molecule/nm^2 with APTES functionalization (Table 1), which was consistent with Tiryaki et al. (2020).

Table 1. Properties of MSA and MSA-NH_3.

As shown in the N_2 adsorption-desorption isotherms given in Fig. 1A, MSA and MSA-NH_3 have similar type IV-like sorption behavior with hysteresis loops, representing the porous aggregates of the particles according to the IUPAC classification. The rapid increase in the adsorption branch at the P/P0 value range of 0.8 to 1.0, combined with the sharp decline in the desorption branch was evidence of the mesoporosity (Ouraipryvan et al., 2009). By the decrease in the surface area after APTES functionalization, the amount of the adsorbed nitrogen of MSA decreased from 610 cm^3/g to 19 cm^3/g at P/P0 = 1, as expected. Tiryaki et al. (2020), pointed out that APTES-modified aerogel samples have lower adsorption capacities as the result of decreased surface areas. The pore size distributions of both MSA and MSA-NH_3 show broad mesopore size distribution in the range of 2.6–18.8 nm represented in Fig. 1A.

3.2. SEM-EDX analysis

The surface morphology of MSA and MSA-NH_3 was examined by SEM. Aerogel samples revealed a porous structure, consisting mostly spherical and agglomerated small particles as shown in Fig. 1B However, while MSA demonstrated dense microstructure, after APTES functionalization, the porous structure, and spherical morphology of MSA became distinct due to the higher tendency of repulsion between organic functional groups like inert CH_3 groups (Cheng et al., 2016). Fig. 1C depicts the EDX results of the samples. The main components of both MSA and MSA-NH_3 were silicon (Si) and oxygen (O) constituting over 30% of the composition, while sodium (Na) was present in minor (below % 1). Following APTES functionalization, the contents of oxygen and magnesium decreased, whereas the contents of silicon (Si), nitrogen (N), and carbon (C) increased (Fig. 1C).

3.2.1. Zeta potential analysis and amount of amine groups on the MSA-NH_3 surface

The zeta potential values of MSA and MSA-NH_3 were assessed under acidic conditions similar to RGJ (pH 3.4) to estimate the variation of surface potential as a function of pH (Table 1). MSA exhibited negative values of zeta potential (−5.11 ± 0.54) due to the presence of a large number of hydroxyl groups on the surface. Following functionalization, APTES molecules react with surface silanol groups (Si-OH) to form stable siloxane bonds (Si–O–Si). The incorporation of amine groups caused a significant change of the zeta potential from negative to high positive values reflecting the presence of a positively charged surface of amine functionalized MSA at acidic pH. Therefore, the zeta potential value of MSA-NH_3 was highly positive (+33.9 mV) in RGJ acidic conditions. Results were consistent with the charge information of amine-functionalized silica materials in the literature (Barczak, 2019; Schulz et al., 2011; Tiryaki et al., 2020).

3.3. FT-IR analysis

MSA and MSA-NH_3 were characterized by FT-IR (Fig. 1D), verifying the presence of functional groups after amino-functionalization. The broadband displayed between 3700 and 3000 cm^{-1}, as well as the peak around 1632 cm^{-1}, were attributed to O—H bonds (Cheng et al., 2016). The asymmetric stretching of the Si – O – Si bonds appeared as a very intense and broadband at around 1014 cm^{-1} and a shoulder around 1200 cm^{-1} wavenumber in MSA and MSA-NH_3 samples. The peaks at 900 cm^{-1} were designated as the stretching vibrations of the surface silanol groups (Si–OH). The symmetric bending of the Si–O–Si bonds was exhibited at around 785 cm^{-1} and this band is present in aerogel samples (Oliveira et al., 2019; Tiryaki et al., 2020). The peak at around 680 cm^{-1} is due to the presence of Mg—O vibrations (Yücel et al., 2016). After the APTES functionalization (Fig. 1D), the peak at 1561 cm^{-1}, attributed to -NH deformation, and moreover, the peaks at 2928 cm^{-1} and 2866 cm^{-1} which correspond to the asymmetric and symmetric vibrations of C—H bonds emerged. The intensity of the peaks between 3700 and 3000 cm^{-1}, and 1632 cm^{-1} attributed to O—H groups decreased due to the reduction in physically absorbed water. The Si–OH bending peak at 900 cm^{-1} disappeared as a result of the APTES molecule reacting with the hydroxyl groups present on the surface of the functionalized MSA. These results were consistent with literature reports (Cheng et al., 2016; Huang et al., 2016; Oliveira et al., 2019; Tiryaki et al., 2020).

3.4. Response surface methodology to optimize RGJ clarification conditions

The effects of independent variables (factors) which are concentration of MSA-NH_3 (A), clarification temperature (B), and clarification time (C) on the responses which are turbidity, acidity, pH, ACN content, TPC and color characteristics ((PC %) and L^*, a^*, and b^* values) were investigated by RSM applying 3-factor Box-Behnken design. The experimental observed and predicted values and ANOVA analysis for responses are given as supplementary information (Table S2 – Tablo S11) and surface diagrams are shown in Fig. 2 The model adequacies were checked by R^2, adjusted-R^2, and predicted-R^2. Non-significant model terms ($p \geq 0.05$) were eliminated from the initial model unless a quadratic or interaction effect including that factor would be significant. The final reduced model was fitted to the experimental data after eliminating the insignificant terms. Multiple regression analysis was applied to experimental data (Table S3 – Tablo S11) and second-order polynomial equations were found to explain the responses given in Table 2 (Eq. (3.1)–(3.9)). The statistical analysis indicates that all proposed second-order polynomial models were indicating an adequate fitting to the actual data, possessing no significant lack of fit and with good R^2 values ($R^2 > 0.90$) for the responses. Additionally, the adequacy

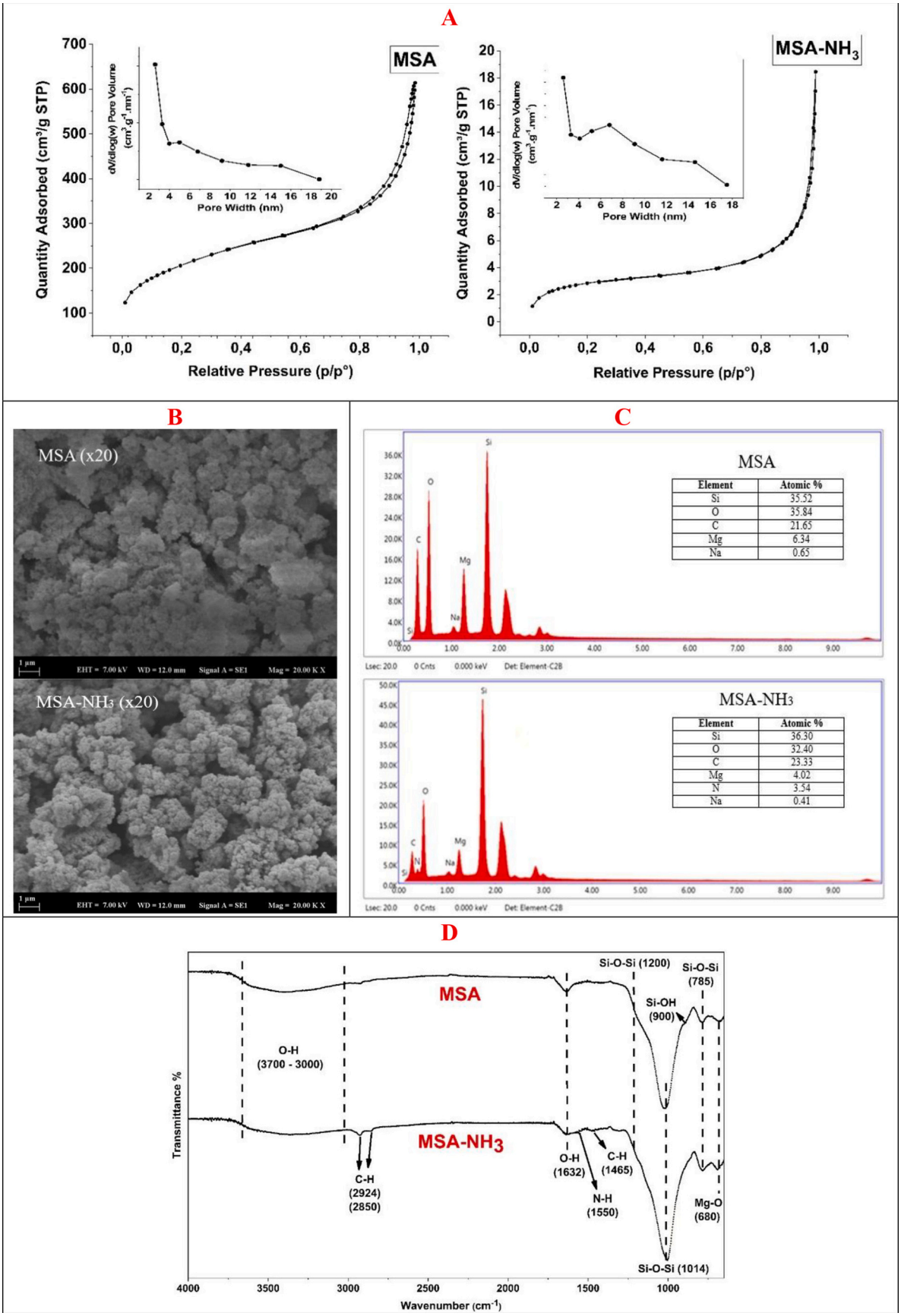


Fig. 1. (A) N_2 adsorption-desorption isotherms and pore size distributions of MSA and MSA-NH_3, (B) SEM images of MSA and MSA-NH_3, (C) EDX spectra of MSA and MSA-NH_3, (D) FT-IR spectra of MSA and MSA-NH_3.

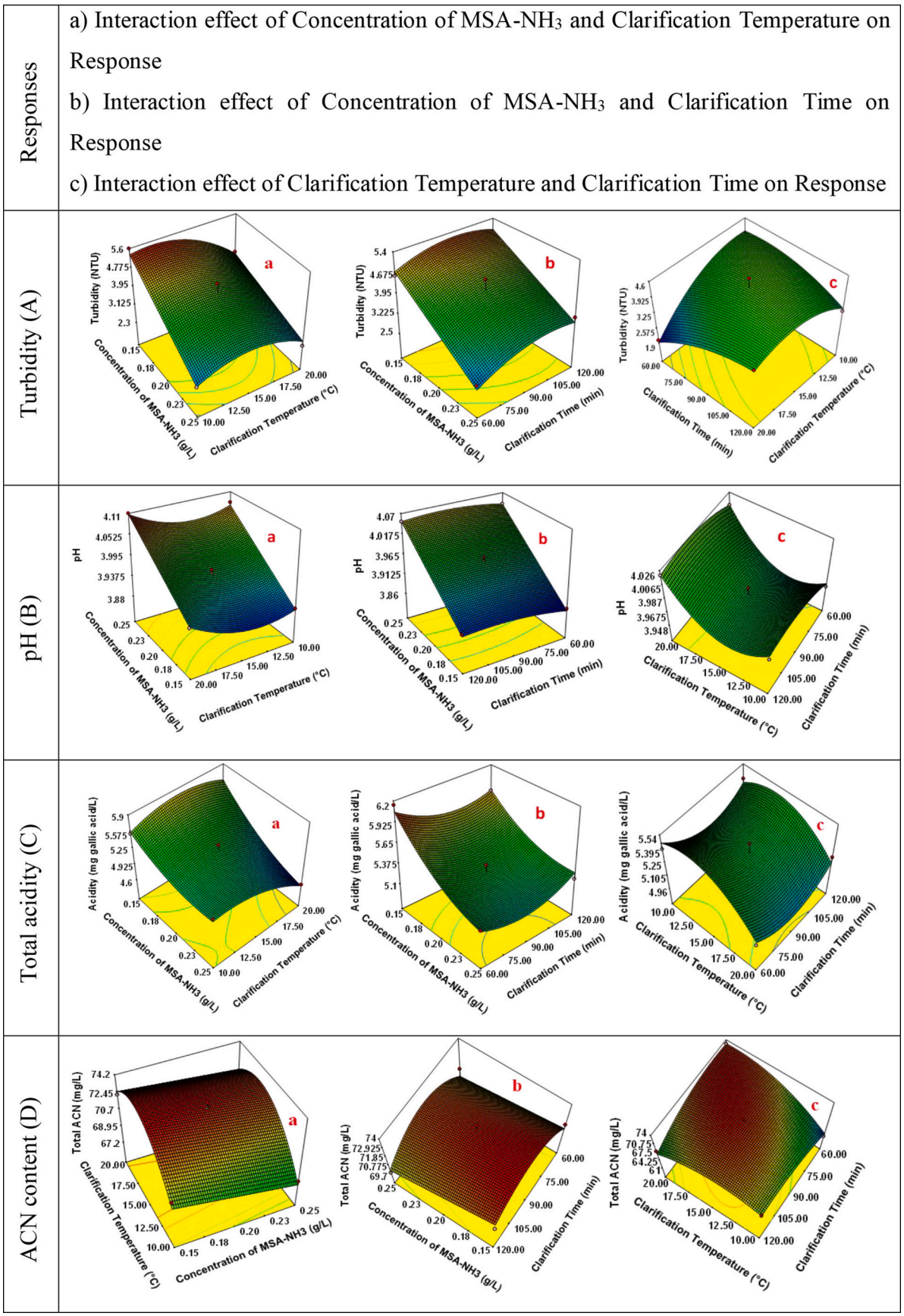


Fig. 2. Surface diagrams of the responses: (A) Turbidity, (B) pH, (C) Total acidity (g/L), (D) ACN content, (E) TPC, (F) PC %, (G) ***L**** value, (H) ***a**** value, (I) ***b**** value.

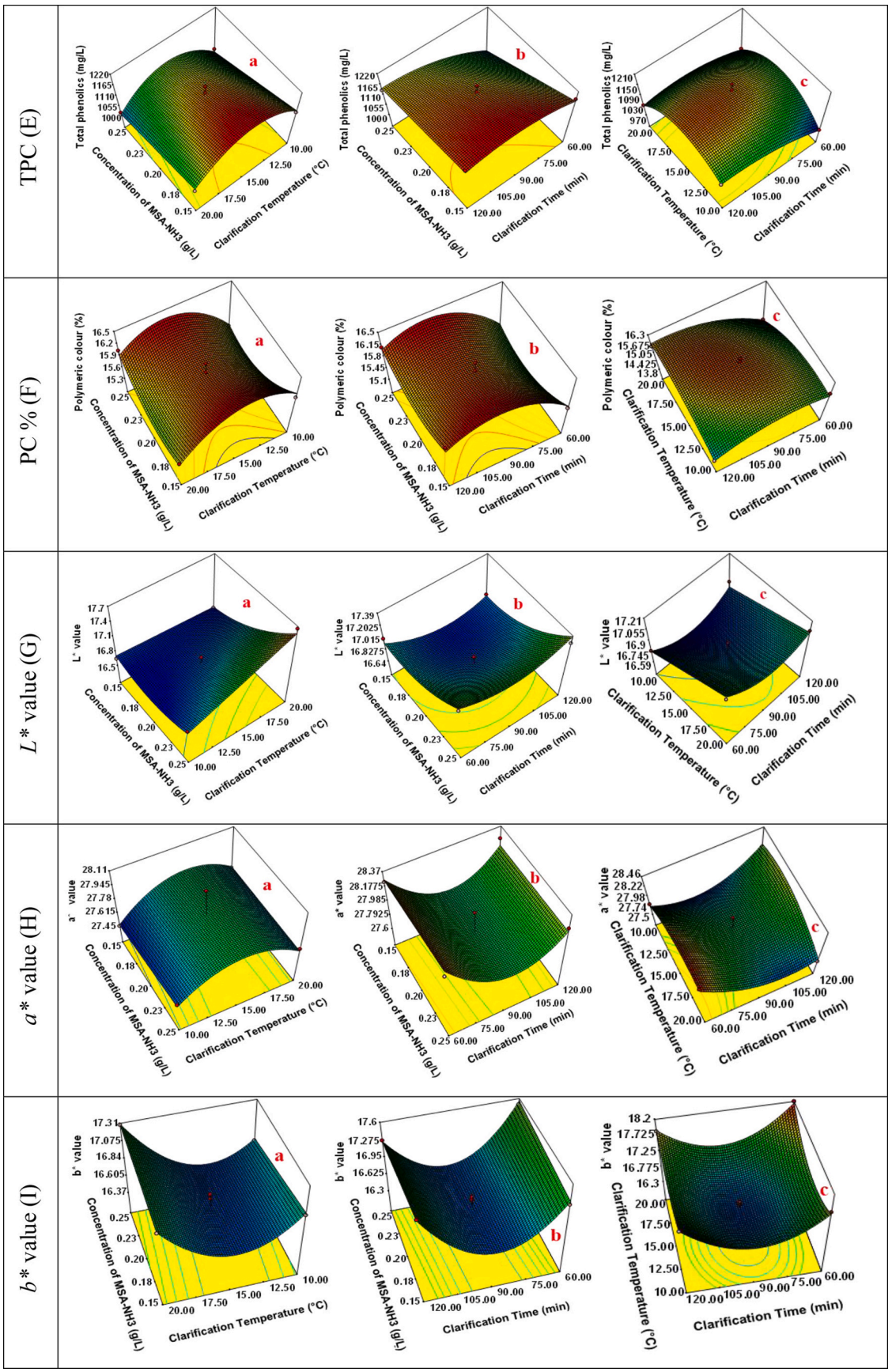


Fig. 2. (*continued*).

Table 2
Second-order polynomial equations of responses.

Responses	Statistical Model Equations	
Turbidity	$Y1 = +4.22–0.99A - 0.40B + 0.24C + 0.36AB + 0.66BC - 0.62B^2–0.34C^2$	Eq. (3.1)
Total acidity	$Y2 = +5.30–0.34A - 0.14B - 0.025C - 0.15AB + 0.075AC + 0.15A^2–0.20B^2 + 0.17C^2$	Eq. (3.2)
pH	$Y3 = +3.97 + 0.085A + 0.020B + 0.007500C + 0.035B^2–0.010C^2$	Eq. (3.3)
ACN content	$Y4 = +73.11–0.79A + 1.84B + 0.17C - 3.09BC - 2.93B^2–2.05C^2$	Eq. (3.4)
TPC	$Y5 = +1167.41–49.30A - 9.30B + 37.33C + 27.90AC - 20.65BC - 106.89B^2–36.19C^2$	Eq. (3.5)
PC %	$Y6 = +15.99–0.066A – 0.006850B + 0.27C + 0.23AB + 0.66BCE + 0.37A^2–0.58B^2–0.61C^2$	Eq. (3.6)
L^* value	$Y7 = +16.77 + 0.25A + 0.18B - 0.026C + 0.20AB + 0.16A^2 + 0.18C^2$	Eq. (3.7)
a^* value	$Y8 = +27.84 + 0.025A + 0.064B - 0.089C - 0.28BC - 0.25B^2 + 0.39C^2$	Eq. (3.8)
b^* value	$Y9 = +16.59 + 0.008750A + 0.16B - 0.022C + 0.088AB - 0.12AC - 0.11BC + 0.45B^2 + 0.81C^2$	Eq. (3.9)

precision (Adeq. Precision) values of all responses related to RGJ properties being >4 and the standard deviation (Std. Dev.) values of errors being <10% indicate that the designed models are appropriate. Therefore, these models can be confidently used to study the changes in turbidity, acidity, pH, ACN content, TPC, and color properties (***L****, ***a****, and ***b**** values and PC %) of RGJ at different clarification conditions.

Table 2**.** Second-order polynomial equations of responses.

3.4.1. Effects of the concentration of MSA-NH$_3$, clarification temperature, and clarification time on responses

Turbidity. Turbidity ranged from 5.60 to 2.05 NTU, which are given in Table S2, and ANOVA analysis (Table S3) exibited that the concentration of MSA-NH$_3$ ($p < 0.0001$) had the highest effect compared to the clarification temperature ($p = 0.0045$) and clarification time ($p = 0.0435$) on turbidity. As can be seen in Eq. (3.1) the concentration of MSA-NH$_3$ has a negative linear effect and clarification temperature has a negative both linear and quadratic effect on turbidity. Meaning that an increase in the concentration of MSA-NH$_3$ and clarification temperature corresponded to a decline in the turbidity. On the other hand, the positive linear effect of the clarification time on turbidity may be associated with the subsequent turbidity, while the negative quadratic effect may be due to the adsorption of the newly formed turbidity component with increasing clarification time. It was observed from the surface diagrams of turbidity (Fig. 2A) that increasing the concentration of MSA-NH$_3$ decreased turbidity under high temperatures and short time conditions. As anticipated, Tastan and Baysal (2015) similarly emphasized that the concentration of chitosan had a negative linear effect on turbidity and increasing the concentration of chitosan, whose adsorption mechanism is based on positive charges similar to MSA-NH$_3$, leads to a reduction in turbidity. However, the quadratic effects of chitosan, process time, and process temperature conditions differ from the MSA-NH$_3$ optimization conditions. These differences can be attributed to the interaction effects of these factors and the distinct surface functional groups of the agents.

However, it was determined that the most important interaction affecting the turbidity value was the temperature and time interaction (q = 0.0019). Effective clarification would take place in the shortest time accompanied by the highest temperature degree when the concentration of MSA-NH$_3$ was kept constant. It was determined that considering turbidity only, the lowest turbidity level (~2 NTU) could be reached if a high concentration of MSA-NH$_3$ (0.25 g MSA-NH$_3$/L RGJ) was used accompanied by either a) low temperature (10 °C) and long-time (118 min) or b) high temperature (18 °C) and short time (63 min) conditions. To achieve effective clarification (~2.58 NTU) in the shortest time (60 min) under conditions with the lowest concentration of MSA-NH$_3$ (0.15 g MSA-NH$_3$/L RGJ), the temperature must be increased to 20 °C which could be a better option considering the industrial clarification at room temperature with saving energy.

Acidity and pH. Linear increases in all system parameters, including the concentration of MSA-NH$_3$, clarification temperature, and clarification time, reduce acidity and increase pH as can be seen in Eq. (3.2) and (3.3). This can be explained by the fact that the MSA-NH$_3$ adsorbs organic acids in RGJ, thus reducing acidity and increasing pH, depending on temperature and time. Surface diagrams of acidity and pH (Fig. 2B and C) also exhibited that with increasing concentration of MSA-NH$_3$, clarification temperature, and clarification time, the pH of RGJ increased considerably and on the contrary, its acidity decreased. Tastan and Baysal (2015), reported a similar decrease in titration acidity of pomegranate juice by clarification with chitosan. Martín-Diana et al. (2009), reported that both linear and logarithmic increase in chitosan concentration significantly increased pH (pH increased from 3.2 to 4.2) in their study to determine the clarification conditions of orange juice with chitosan. In our study, it would be appropriate to perform clarification with 0.15 g MSA-NH$_3$/L RGJ, 20 °C, and 60 min conditions previously suggested by the model for turbidity, to obtain RGJ with low turbidity, high acidity, and low pH.

Total monomeric ACN content and TPC. Phenolics are functional compounds that have an antioxidant effect in fruit juices but also form the main turbidity factors of fruit juices binding with proteins. Although it is necessary to remove them by clarification, phenolic compounds, especially anthocyanins, which have high bioavailability in line with consumer needs, should be present and remain unadsorbed in fruit juice at a certain level (Çapanoğlu Güven et al., 2010).

Linear increases in the concentration of MSA-NH$_3$, logarithmic increases in clarification temperature and time, and finally the interaction of temperature and time have a decreasing effect on the total monomeric anthocyanin and total phenolic compounds (Eq. 3.4 and 3.5; Fig. 2D and E). However, it was also observed that the linear increase in temperature has an increasing effect on the amount of total monomeric ACN in RGJ (Eq. 3.4). Fig. 2D indicates that the clarification temperature has a significant effect on the adsorption of ACNs, considering the interactions with the concentration of MSA-NH$_3$ and clarification time. It was determined that the amount of ACNs decreased to 61.97 mg/L under low temperature (10 °C) and short time (60 min) conditions, especially when the concentration of MSA-NH$_3$ was fixed at a moderate level (0.2 g MSA-NH$_3$ /L RGJ).

The effect of increasing temperature on increasing the amount of ACNs is explained for several reasons in the literature: a) The fact that Mg metal in the structure of MSA-NH$_3$ increases ACN stability with a bentonite-like copigmentation effect, due to the dominant ACN content in grape juice contains hydroxyl groups, b) the high copigmentation effect at pH levels that reach around 4 with the effect of clarification, c) the dominant ACNs in grape juice are in polymeric structure and fragmented into monomeric structure, (Özkan, 2014) d) extraction of complex ACNs with the effect of temperature (Alighourchi et al., 2008) or e) The low amount of ascorbic acid, one of the most important compounds that accelerates the degradation of ACNs, in grape juice (Özkan, 2005). Therefore, in our study, considering the positive effect of the linear increase in temperature on ACN and the importance of the interaction of clarification temperature with the clarification time, the clarification time should be shortened to reduce the degradation and adsorption level of various ACNs in case of high-temperature clarification. As depicted in Fig. 2E, the concentration of MSA-NH$_3$ and clarification time emerge as the most significant factors affecting TPC. Nevertheless, the interactions among the concentration of MSA-NH$_3$, clarification temperature, and clarification time parameters were statistically insignificant ($p > 0.05$).

The conditions recommended by the Box-Behnken model, specifically 0.15 g MSA-NH$_3$/L RGJ, 20 °C, and 60 min, for minimizing turbidity also correspond to the maximum ACN content and high phenolic content. It has been determined that under these conditions, an effective clarification of RGJ with low turbidity and high acidity will be achieved with also high (73.68 mg/L) ACN content and high (1203 mg/

L) phenolic content.

Color characteristics : L^*, a^*, and b^* values and PC%.

Color is a crucial quality factor in grape juices, impacting consumer sensory acceptance. The appealing red color of grape juice primarily results from ACN presence. The stability of these ACNs is influenced by both internal factors like grape composition and external factors such as grape juice processing conditions. Measuring total monomeric ACN content along with polymeric color is very useful for assessing the color quality of ACN-rich juices during processing (Danişman et al., 2015).

The linear increase in the clarification temperature and the concentration of MSA-NH_3, as well as the logarithmic increase in the clarification time, lead to an increase in the L^* (whiteness), a^* (redness), and b^* (yellowness) values while decreasing in the PC % (Eq. 3.6–3.9). This can be explained by the adsorption of green and blue colored compounds, which are characterized by negative a^* and b^* values, in grape juice as a result of the increasing clarification temperature, the concentration of MSA-NH_3, and prolonged clarification time.

It was determined that the interaction of temperature and time is the most significant factor affecting the total monomeric ACN content ($p <$

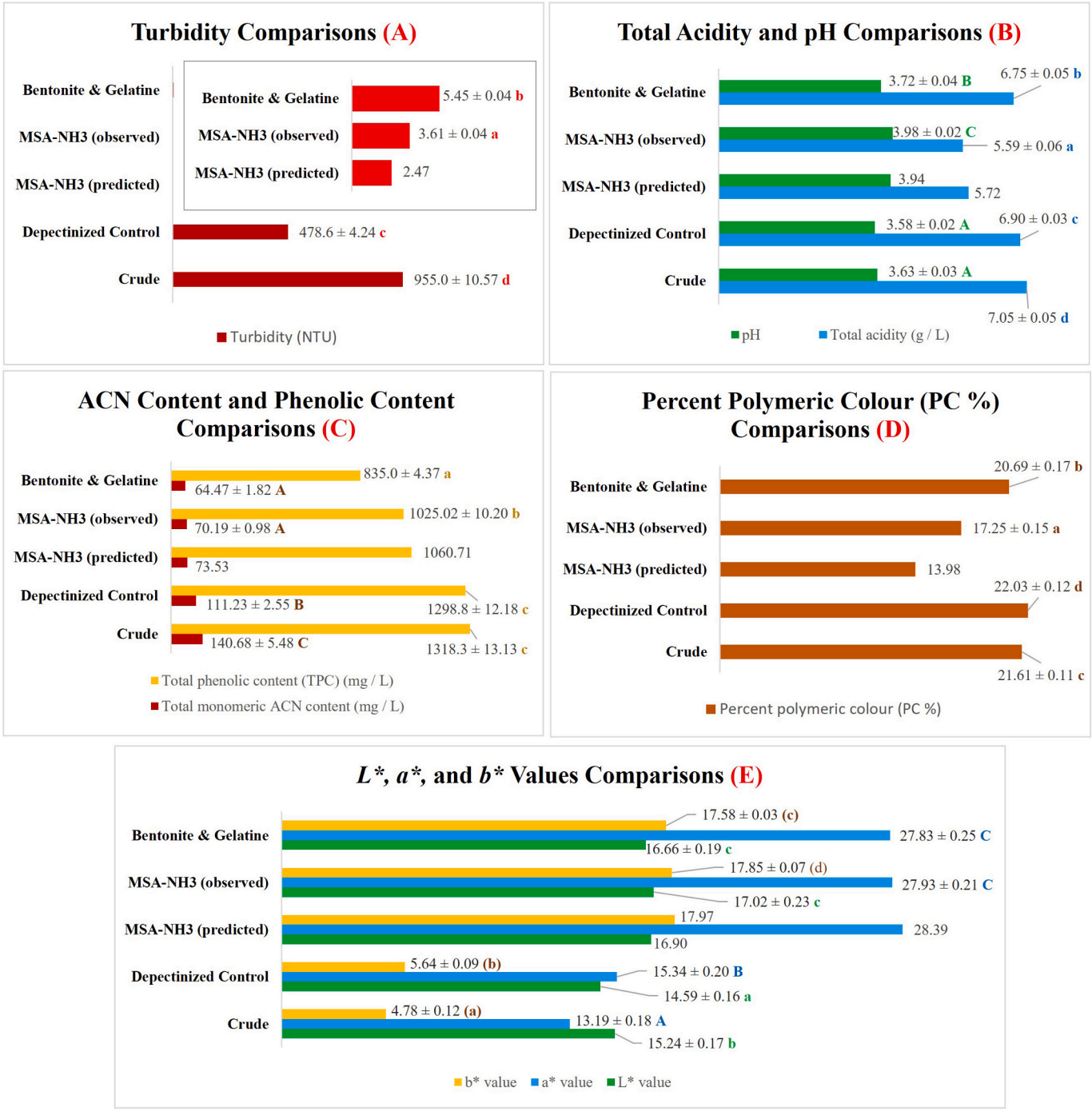


Fig. 3. Comparison of predicted and observed response values clarified by MSA-NH_3 with BGC response values: (A) Turbidity comparison, (B) Total acidity and pH comparison, (C) ACN content and phenolic content comparison, (D) Percent polymeric color (PC %) comparison, (E) L^*, a^*, and b^* values comparison. *V*alues were expressed as means ± S.D. ($n = 3$). Different lowercase and/or uppercase letters within the same bar chart indicate significant differences among treatments ($P <$ 0.05), according to Tukey's test, except for turbidity, which was analyzed using Games-Howell's test.

0.0001), the a^* value ($p = 0.0052$), and PC % ($p = 0.0015$), which are essential indicators of the natural color of clarified red grape juice (Table S6, S8, and S10). When examining the surface graphs (Fig. 2D, F, and H) and equations (Eq. 3.4, 3.6, and 3.8), it becomes evident that uncontrolled increases in temperature and time parameters result in a higher degradation level of ACNs. This, in turn, has a detrimental effect on the red color and may lead to the formation and/or release of brown-colored compounds. The conditions recommended by the Box-Behnken model for turbidity, including 0.15 g MSA-NH_3/L, 20 °C, and 60 min, have been found not only provide the maximum total monomeric ACN content (73.68 mg/L) but also to be conducive to a positive a^* value and a low PC%.

3.5. Confirmative tests and comparing with BGC

In this study, desirability functions (0.790) were developed for the criteria of minimum turbidity and maximum acidity and all of the other responses in range value. The proposed optimum conditions for the clarification of RGJ were found to be 0.16 g MSA-NH_3/L RGJ, at 20 °C, and 60 min. The predictive accuracy of the model equations was validated by testing it under the recommended optimum conditions, showing good agreement between predicted and observed response values. The predicted response values observed response values and their comparison with industrial BGC response values are exhibited in Fig. 3 (A) – (E).

The changes in turbidity during the clarification process using MSA-NH_3 and BGJ are illustrated in Fig. 3(A). The initial phase of clarification involved depectinization, which decreased the turbidity of RGJ from 955 NTU (in unclarified crude RGJ) to 478.60 NTU (in depectinized control RGJ). Pectinase inevitably reduced the turbidity by facilitating pectin degradation, consistent with the findings of Lee et al. (2006). MSA-NH_3 exhibited strong adsorption of turbidity elements in RGJ compared to the BGC. On the other hand, clarification with the BGC resulted in higher losses in total phenolic components of RGJ (35.94%) compared to those clarified with MSA-NH_3 (21.08%), as depicted in Fig. 3(C). The literature attributes the decline of negatively charged phenolic compounds to positively charged gelatin and emphasizes the diverse adsorption mechanism of gelatin-based on phenolic type, hydrophobicity, and molecular weight (Dıblan & Özkan, 2021; Özkan, 2014). Erkan-Koç et al. (2015) attributed the significant reduction in TPC by gelatin to the high isoelectric point (pI) of gelatin in pomegranate juice, which is 7.0. However, despite gelatin being rich in hydrophobic prolyl units with a high affinity for haze-active polyphenols, its adsorption performance for polyphenols is low when the molecular weight of the polyphenols is below 500 Da (Turfan, Türkyılmaz, Yemis, & Özkan, 2011). Among the polyphenols, tannins are the most important ones for turbidity and sediment formations (Goertges & Dickmann, 1982). The monomer polyphenols, including flavonols and flavanols, with MW lower than 500 U, tend to oxidize and polymerize and eventually convert to tannins, so that they have more ends that can bind to HA proteins, thus forming large HA polymers (Wang & Ye, 2021). Although their ratios vary depending on the grape variety, the dominant flavan-3-ols in grape varieties were determined to be catechin and epicatechin (Iacopini et al., 2008; Yilmaz & Toledo, 2004). MSA-NH_3 could be adsorbed flavan-3-ols, such as catechin or epicatechin (<500 Da), which contribute to turbidity, unlike gelatin. Balík et al. (2007) reported a 72% and 73% decrease, respectively, in the amount of catechin and epicatechin (290 Da), monomer flavan-3-ols, when egg albumin was used, whereas these values were determined to be 0% and 3% for gelatin. The outstanding adsorption performance of MSA-NH_3 has been mostly attributed to the high positively charged multiple amine functional groups of MSA-NH_3. Dıblan and Özkan (2021) stated that potassium caseinate exhibits more positive charges due to the amine content than ordinary casein, resulting in a greater affinity for RGJ phenolics and consequently lower turbidity compared to casein and other protein-based clarifying agents (gelatin and albumin). However, the clarification performance of chitosan, whose clarification mechanism also relies on positive charges, has shown conflicting results in the literature when compared to bentonite and gelatin (Dıblan & Özkan, 2021; Özkan, 2014; Tastan & Baysal, 2015). Özkan (2014) noted that hydrophilic chitosan reduces the turbidity level of grape juice less effectively than bentonite, gelatin, and other clarification agents, as it removes hydrophobic phenolic compounds in smaller amounts. MSA-NH_3 may not only engage in adsorption with positive charges but also enable the adsorption of hydrophobic phenolics due to the hydrophobic groups in its structure, in contrast to chitosan. Consequently, it is hypothesized to exhibit superior clarification performance compared to the BGC, while preserving the phenolic content due to effecting only haze-active components. In accordance with our study, Türkyılmaz et al. (2020) found that despite pomegranate juice clarified with chitosan (CH) and xanthan gum (XG) showing a higher phenolic content, the turbidity of pomegranate juice clarified with 'CH + XG' was lower compared to that clarified with other agents. They associated this phenomenon with these agents that simultaneously link and remove haze-active proteins in PJ, thereby these agents also linked and eliminated fewer phenolic compounds. Silica gel is consistently employed to eliminate HA proteins for minimizing haze formation (Wang & Ye, 2021). According to McKeown and Nock (1996), the optimal pore size for silica hydrogel ranges from 3 to 12 nm. Fernyhough et al. (1994) found that applying 75 g/hL of silica could extend the shelf life of beer by 3–6 months, and utilizing silica twice doubles the extension of shelf life. It is conceivable that MSA-NH_3, with its mesoporous pore size (4.91 nm), also adsorbed HA proteins, thereby further decreasing turbidity while conserving non-HA polyphenols.

Organic acids and pH have also played a role in haze formation (Batista et al., 2010). In our study, the BGC better maintained the organic acid profile of grape juice compared to MSA-NH_3, as can be seen in Fig. 3(B). Türkyilmaz et al. (2012) explained the decrease in titratable acidity by suggesting that acids might be removed from the beverage with the gelatine flocs. On the other hand, Chatterjee et al. (2004) found that the clarification of grape juice with chitosan decreased the titration acidity more than bentonite-gelatine. Martín-Diana et al. (2009) attributed the increase in pH value to the acid-binding property of chitosan, a polycationic clarifying agent, which may have a mechanism similar to MSA-NH_3. Organic acids, which provide a natural protective effect in fruit juices, must be above a certain value depending on the type of fruit juice to provide the appropriate brix/acid ratio at the same time. Despite MSA-NH_3 showing higher adsorption of organic acids, the acidity value of RGJ clarified by MSA-NH_3 aligns with the requirement of "must be at least 2.0 g/L" as specified in the TS 3632 Grape Juice Standard. However, there is no restriction in the standard for pH value.

Depectinization decreased the ACN content of the crude RGJ sample, as depicted in Fig. 3(C) (depectinized control sample). Clarification with the BGC caused to higher losses in monomeric ACN content (42.04%) compared to those clarified with MSA-NH_3 (36.90%). In line with our findings, Dıblan and Özkan (2021) observed the greatest loss of ACNs in RGJ clarified with gelatin, and bentonite, both alone and in combination. The literature highlights the role of negatively charged bentonite in the reduction of positively charged ACNs (Gómez-Plaza et al., 2000; Ribéreau-Gayon et al., 2006). On the other hand, due to its positive charge, MSA-NH_3 is thought to have a lesser impact on anthocyanin reduction as it lacks electrostatic interaction with positively charged anthocyanins, unlike bentonite. It has also been reported that gelatin forms large flocs by binding with high molecular weight polyphenols (>500 Da), resulting in the removal of ACNs along with these large flocs. Since catechin and epicatechin have a molecular weight below 300 Da, it is unlikely that they would interact with gelatin (Orhan Dereli et al., 2023; Turfan, Türkyılmaz, Yemis, & Özkan, 2011). On the contrary, in our study, the reduced loss of ACN with MSA-NH_3 may be attributed to the fact that MSA-NH_3, unlike BGC, can bind to low molecular weight polyphenols, forming small flocs that do not eliminate ACNs. Various studies have reported that after clarification with albumin, there is a

greater decrease in epicatechin and catechin ratios compared to gelatin, but there is less loss in anthocyanins because the flocs with these monomer polymers flavan-3-ols are smaller (Balík et al., 2007; Özkan, 2014; Puškaš & Miljić, 2012).

The percent polymeric color (PC %) is a measure of the resistance of ACNs to bisulfite bleaching and shows the degree of ACN polymerization and browning (Turfan, Türkyilmaz, Yemi, & Özkan, 2011). The potential mechanism for polymerization involves the reaction of monomeric ACNs condensed tannins (CTs) or flavan-3-ols, such as catechin or epicatechin. Multiple phenolic hydroxyl groups of CTs lead to the formation of complexes with ACNs (Türkyilmaz & Özkan, 2014). Typically, untreated fruit juices aim for a polymeric color ratio close to 10%, with exceptions noted (Çapanoğlu Güven et al., 2010). However, once the juice is obtained from fruits and vegetables, this value will increase as a result of the formation of ACN and tannin complexes as well as the activities of peroxidases and polyphenoloxidases (Hager et al., 2008). Additionally, the depectinization process, conducted at 50 °C for a specific duration before grape juice clarification, deactivates enzymes responsible for anthocyanin breakdown while transferring skin anthocyanins to the juice and leads to an increase in the polymeric color ratio (Özkan, 2014). In our study, we observed high PC % values in both pressed and depectinized RGJs, as depicted in Fig. 3(D), consistent with this information. Following clarification, MSA-NH_3 exhibited superior adsorption of dark-coloured undesirable compounds compared to the BGC, especially when evaluating PC %. Türkyilmaz et al. (2012) determined that PC values significantly decreased in black carrot juice (BCJ) samples after the clarification with bentonite and gelatin–kieselsol. They explained that the decrease in PC may result from the interactions among bentonite, protein, and polyphenols, and concluded that the floc formed by adsorption could lead to the removal of brown-colored pigments. Orhan Dereli et al. (2023) observed a decrease in polymeric color in pomegranate juice with the use of bentonite, gelatine, and kiselsol. They attributed this decrease to the potential of bentonite to either adsorb the brown-colored compounds or remove the polyphenol oxidase (PPO) enzyme from the juice. Dıblan and Özkan (2021) determined that the lowest PC value was observed with bentonite and gelatin clarification. The impact of MSA-NH_3 on PC components may be associated with different mechanisms: it can directly remove PC components and/or PPOs by adsorption, similar to bentonite and chitosan, and it can indirectly eliminate PC by adsorbing flavan-3-ols and polymerized tannins that generate PC through the formation of flocs with ACN, similar to the mechanism of albumin.

Depectinization increased the reflectance color values (L^*, a^*, and b^*) of the crude RGJ sample, as depicted in Fig. 3(E) (depectinized control sample). Pectinase has the capability to break down long and complex pectin molecules, leading to the release of anthocyanins and consequently enhancing the redness of the juice (Türkyilmaz et al., 2012). Furthermore, the enzymatic hydrolysis of pectin can result in a clearer juice with higher lightness (Mirzaaghaei et al., 2016). The increase after clarification in the reflectance color values (L^*, a^*, and b^*) of RGJ samples was observed to be similar for both aerogel and bentonite-gelatin applications, consistent with findings in the literature (Rommel et al., 1990; Turfan et al., 2011). Balík et al. (2007) observed an increase in the proportion of polymeric forms of anthocyanins contributing to the final coloration of red wine as well as an enhancement in the intensity of the red tone (a^* value), across all types of clarified agent treatments. Rommel et al. (1990) explained that the increases in L^* and b^* values were associated with the particles susceptible to browning that were removed by the gelatin used for the clarification of pomegranate juice. During clarification, Al and Mg, which are present in the structure of sepiolite and bentonite, may be released into the juice, causing copigmentation. This phenomenon can lead to an increase in the amounts of anthocyanin in PJ and RGJ (Mirzaaghaei et al., 2016; Özkan, 2014; Wu et al., 2024). Furthermore, the copigmentation effect is heightened at a pH of around 4 (Özkan, 2014). In our study, even though clarification agents remove ACNs during the clarification process, Mg in the structure of MSA-NH_3 may be released into the juice, causing more copigmentation compared to bentonite. This effect could be attributed to the pH being closer to 4 due to increased adsorption of organic acids. Furthermore, certain amounts of anthocyanins may become trapped in complexes formed between gelatin flocs during the clarification process, resulting in reduced redness (Türkyilmaz et al., 2012). Consequently, this might result in a lesser decrease in the amount of ACN compared to BGC, and the a^* value representing redness could be slightly higher than BGC.

4. Conclusions

The mesoporous and spherical-shaped amine-functionalized magnesium silicate aerogel (MSA-NH_3), which exhibits a high positive charge (+33.9 mV) under RGJ acidic conditions, was successfully synthesized. The surface area and pore volume of MSA-NH_3 decreased with the acquisition of more functional groups, while its pore diameter increased to 6.29 nm, and the amount of amine groups attached to the aerogel surface was calculated as 61.44 ± 0.05 molecules/nm^2 with APTES functionalization. The emergence of peaks at 1561 cm^{-1}, 2928 cm^{-1}, and 2866 cm^{-1}, attributed to -NH deformation, asymmetric, and symmetric vibrations of C—H bonds, respectively, along with the reduction in peaks of physically absorbed water between 3700 and 3000 cm^{-1}, and at 1632 cm^{-1}, revealed the successful functionalization of MSA-NH_3 with APTES. Consequently, MSA-NH_3 still exhibited a highly porous structure (92%). The proposed optimal conditions for RGJ clarification were determined to be 0.16 g MSA-NH_3/L RGJ, at 20 °C, and 60 min, according to the Box-Behnken model. Confirmatory tests of these conditions revealed that MSA-NH_3 effectively clarified RGJ, resulting in low turbidity (3.61 NTU) and maximum total monomeric ACN content (70.19 mg/L), high TPC (1025.02 mg/L), positive a^* value (27.93), and low PC % (17.85%) compared to BGC, which exhibited turbidity of 5.45 NTU, total monomeric ACN content of 64.47 mg/L, TPC of 835.00 mg/L, a^* value of 27.83, and PC % of 20.69%. Conversely, BGC better maintained the acidity value (6.75 g/L and 5.59 g/L, respectively) and pH (3.72 and 3.98) of RGJ compared to MSA-NH_3. Even so, the acidity of RGJ clarified by MSA-NH_3 still meets the standard. In our study, we hypothesize that MSA-NH_3 demonstrates superior clarification performance compared to BGC, while better preserving phenolic content and ACNs by targeting only haze-active components. Although our study demonstrates that the use of MSA-NH_3 is a promising and alternative method for clarifying RGJ, the fact that aerogel production is still at the laboratory stage and there are no comparative studies regarding its adsorption potential poses the limitation in determining the real potential application of this field. In future studies, a comprehensive investigation should be conducted to explore: (I) the clarification potential of different beverages with varying haze characteristics; (II) the effects of MSA-NH_3 on individual phenolic and anthocyanin compounds, as well as other haze-active compounds and organic acids; (III) the impacts of MSA-NH_3 on toxic components such as heavy metals, pesticides, histamine-like biogenic amines, and microorganisms; (IV) the potential for reuse in the aerogel clarification process, including the number of cycles and available capacities; (V) the environmental impacts and sustainability of aerogel clarification performance compared to alternative agents; and (VI) the exploration of the potential of aerogel clarification through a scale-up approach. This comprehensive approach will lead to a more accurate and comprehensive understanding of silica-aerogel based materials potential in the clarification industry.

CRediT authorship contribution statement

Ilkay Turhan Kara: Writing – review & editing, Writing – original draft, Visualization, Methodology, Investigation, Conceptualization. **Sevil Yücel:** Writing – review & editing, Writing – original draft, Supervision, Resources, Project administration, Conceptualization.

Muhammet Arici: Writing – review & editing, Writing – original draft, Supervision, Conceptualization.

Declaration of competing interest

The authors declare that they have no known competing financial interests or personal relationships that could have appeared to influence the work reported in this paper.

Data availability

Data will be made available on request.

Acknowledgements

This study is in part of Miss Turhan Kara's doctorate thesis and funded by "Yildiz Technical University Scientific Research Projects Office" Turkey (Grant FDK-2017-3139). We, as the author of this manuscript, would like to acknowledge the following contributions: All laboratorial analyses were carried out by Ilkay Turhan Kara under the supervision of Sevil Yucel and Muhammed Arici. The manuscript was written by Ilkay Turhan Kara and edited by Sevil Yucel and Muhammed Arici. The authors thank Tekirdag Viticulture Research Institute (Republic of Turkey Ministry of Agriculture and Forestry) in Tekirdag, Turkey for providing the RGJs, pectinase enzyme, and industrial clarification agents which are gelatine and bentonite.

Appendix A. Supplementary data

Supplementary data to this article can be found online at https://doi.org/10.1016/j.foodchem.2024.140132.

References

Alighourchi, H., Barzegar, M., & Abbasi, S. (2008). Anthocyanins characterization of 15 Iranian pomegranate (Punica granatum L.) varieties and their variation after cold storage and pasteurization. *European Food Research and Technology, 227*(3), 881–887. https://doi.org/10.1007/s00217-007-0799-1

Alnaief, M., & Smirnova, I. (2010). Effect of surface functionalization of silica aerogel on their adsorptive and release properties. *Journal of Non-Crystalline Solids, 356*(33–34), 1644–1649. https://doi.org/10.1016/j.jnoncrysol.2010.06.027

Arslan Kulcan, A., Öziyci, H. R., Tetik, N., & Karhan, M. (2015). Changes in turbidity, total phenolic and anthocyanin contents of clear red grape juice during processing. *GIDA / THE JOURNAL OF FOOD, 40*(6), 311–317. https://doi.org/10.15237/gida.gd15029

Balík, J., Kyseláková, M., Veverka, J., Tříska, J., Vrchotová, N., Totušek, J., & Lefnerová, D. (2007). *The effect of clarification on colour* (Concentration of Anthocyanins and Polyphenols in Red Wine).

Barczak, M. (2019). Amine-modified mesoporous silicas: Morphology-controlled synthesis toward efficient removal of pharmaceuticals. *Microporous and Mesoporous Materials, 278*, 354–365. https://doi.org/10.1016/j.micromeso.2019.01.012

Batista, L., Monteiro, S., Loureiro, V. B., Teixeira, A. R., & Ferreira, R. B. (2010). Protein haze formation in wines revisited. The stabilising effect of organic acids. *Food Chemistry, 122*(4), 1067–1075. https://doi.org/10.1016/j.foodchem.2010.03.076

Canbaş, A., Deryaoğlu, A., & Cabaroğlu, T. (1996). ÜLKEMİZİN ÖNEMLİ BAZI ÜZÜM ÇEŞİTLERİNDEN KABARCIKLI ÜZÜM SUYU ÜRETİMİ I. 1992 YILI DENEMELERİ. *GIDA, 21*(6), 313–319.

Çapanoğlu Güven, E., Toydemir Otkun, G., Boyacıoğlu, D., Teknik Üniv, İ., Fakültesi, K.-M., Mühendisliği Bölümü, G., & tarihi, G.. (2010). FLAVONOİDLERİN BİYOYARARLILIĞINI ETKİLEYEN FAKTÖRLER FACTORS AFFECTING BIOAVAILABILITY OF FLAVONOIDS. *In Derleme / Review GIDA*, (5).

Cemeroğlu, B. (2004). *Meyve ve sebze işleme teknolojisi (Cilt 1–2)*. Ankara: Başkent Klişe Matbaacılık.

Chatterjee, S., Chatterjee, S., Chatterjee, B. P., & Guha, A. K. (2004). Clarification of fruit juice with chitosan. *Process Biochemistry, 39*(12), 2229–2232. https://doi.org/10.1016/j.procbio.2003.11.024

Chen, K., Feng, Q., Ma, D., & Huang, X. (2021). Hydroxyl modification of silica aerogel: An effective adsorbent for cationic and anionic dyes. *Colloids and Surfaces A: Physicochemical and Engineering Aspects, 616*. https://doi.org/10.1016/j.colsurfa.2021.126331

Cheng, Y., Xia, M., Luo, F., Li, N., Guo, C., & Wei, C. (2016). Effect of surface modification on physical properties of silica aerogels derived from fly ash acid sludge. *Colloids and Surfaces A: Physicochemical and Engineering Aspects, 490*, 200–206. https://doi.org/10.1016/j.colsurfa.2015.11.055

Ciesielczyk, F., Krysztafkiewicz, A., & Jesionowski, T. (2004). *INFLUENCE OF PRECIPITATION PARAMETERS ON PHYSICOCHEMICAL PROPERTIES OF MAGNESIUM SILICATES. In Physicochemical problems of mineral processing. 38*.

Danişman, G., Arslan, E., & Toklucu, A. K. (2015). Kinetic analysis of anthocyanin degradation and polymeric colour formation in grape juice during heating. *Czech Journal of Food Sciences, 33*(2), 103–108. https://doi.org/10.17221/446/2014-CJFS

Dıblan, S., & Özkan, M. (2021). Effects of various clarification treatments on anthocyanins, color, phenolics and antioxidant activity of red grape juice. *Food Chemistry, 352*. https://doi.org/10.1016/j.foodchem.2021.129321

Ek, S., Iiskola, E. I., & Niinistö, L. (2003). Gas-phase deposition of aminopropylalkoxysilanes on porous silica. *Langmuir, 19*(8), 3461–3471. https://doi.org/10.1021/la020869q

Erkan-Koç, B., Türkyilmaz, M., Yemiş, O., & Özkan, M. (2015). Effects of various protein- and polysaccharide-based clarification agents on antioxidative compounds and colour of pomegranate juice. *Food Chemistry, 184*, 37–45. https://doi.org/10.1016/j.foodchem.2015.03.064

Fernyhough, R., McKeown, I., & McMurrough, I. (1994). Beer stabilization with silica gel. *Brew Guard, 123*(10), 44–50.

Ferreira, R. B., Piçarra-Pereira, M. A., Monteiro, S., Loureiro, V. B., & Teixeira, A. R. (2001). The wine proteins. *Trends in Food Science & Technology, 12*(7), 230–239. https://doi.org/10.1016/S0924-2244(01)00080-2

Ghahremani, P., Vakili, M. H., & Nezamzadeh-Ejhieh, A. (2021). Optimization of Pb(II) removal by a novel modified silica aerogel using quince seed mucilage with response surface methodology. *Journal of Environmental Chemical Engineering, 9*, 2213–3437. https://doi.org/10.1016/j.jece.2021.106648

Ghods, B., Rezaei, M., & Meshkani, F. (2016). Synthesis of nanostructured magnesium silicate with high surface area and mesoporous structure. *Ceramics International, 42*(6), 6883–6890. https://doi.org/10.1016/j.ceramint.2016.01.073

Giusti, M. M., & Wrolstad, R. E. (2001). Characterization and measurement of anthocyanins by UV-visible spectroscopy. *Current protocols in food. Analytical Chemistry, 00*(1). https://doi.org/10.1002/0471142913.FAF0102S00. F1.2.1-F1.2.13.

Goertges, S., & Dickmann, H. (1982). [prevention of cloudiness in apple juices.] Wie schuetzt man Apfelsaefte vor Nachtruebungen. *Fluessiges Obst, 49*, 584–587.

Gómez-Plaza, E., Gil-Muñoz, R., López-Roca, J. M., De La Hera-Orts, M. L., & Martínez-Cultíllas, A. (2000). Effect of the addition of bentonite and Polyvinylpolypyrrolidone on the colour and long-term stability of red wines. *Journal of Wine Research, 11*(3), 223–231. https://doi.org/10.1080/713684236

Gurav, J. L., Jung, I. K., Park, H. H., Kang, E. S., & Nadargi, D. Y. (2010). Silica aerogel: Synthesis and applications. *Journal of Nanomaterials, 2010*. https://doi.org/10.1155/2010/409310

Hager, T. J., Howard, L. R., & Prior, R. L. (2008). Processing and storage effects on monomeric anthocyanins, percent polymeric color, and antioxidant capacity of processed blackberry products. *Journal of Agricultural and Food Chemistry, 56*(3), 689–695. https://doi.org/10.1021/jf071994g

Hatamikia, M., Sani, A. M., & Zomorodi, S. (2013). Effect of different clarifying agents on the physico-chemical properties of grape juice concentrate regular paper. *In RRBS, 7*(1).

Howarter, J. A., & Youngblood, J. P. (2006). Optimization of silica silanization by 3-aminopropyltriethoxysilane. *Langmuir, 22*(26), 11142–11147. https://doi.org/10.1021/la061240g

Hozhabr Araghi, S., & Entezari, M. H. (2015). Amino-functionalized silica magnetite nanoparticles for the simultaneous removal of pollutants from aqueous solution. *Applied Surface Science, 333*, 68–77. https://doi.org/10.1016/j.apsusc.2015.01.211

Huang, Y. D., Gao, X. D., Gu, Z. Y., & Li, X. M. (2016). Amino-terminated SiO2 aerogel towards highly-effective lead (II) adsorbent via the ambient drying process. *Journal of Non-Crystalline Solids, 443*, 39–46. https://doi.org/10.1016/j.jnoncrysol.2016.04.007

Iacopini, P., Baldi, M., Storchi, P., & Sebastiani, L. (2008). Catechin, epicatechin, quercetin, rutin and resveratrol in red grape: Content, in vitro antioxidant activity and interactions. *Journal of Food Composition and Analysis, 21*(8), 589–598. https://doi.org/10.1016/J.JFCA.2008.03.011

Ihsanullah, I., Sajid, M., Khan, S., & Bilal, M. (2022). Aerogel-based adsorbents as emerging materials for the removal of heavy metals from water: Progress, challenges, and prospects. In *, 291. Separation and purification technology*. Elsevier B. V. https://doi.org/10.1016/j.seppur.2022.120923.

Jung, H. S., Moon, D. S., & Lee, J. K. (2012). Quantitative analysis and efficient surface modification of silica nanoparticles. *Journal of Nanomaterials, 2012*. https://doi.org/10.1155/2012/593471

Kandylis, P. (2021). Grapes and their derivatives in functional foods. In *, 10. Foods*. MDPI AG. https://doi.org/10.3390/foods10030672. Issue 3.

Kara, İ. T., Yücel, S., & Arici, M. (2020). Optimization aging parameters of mg silica aerogel using box-behnken approach. *Journal of Nano Research, 62*, 31–46. https://doi.org/10.4028/www.scientific.net/jnanor.62.31

Kemp, B., Marangon, M., Curioni, A., Waters, E., & Marchal, R. (2021). New directions in stabilization, clarification, and fining. In *Managing wine quality: Volume 2: Oenology and wine quality* (pp. 245–301). Elsevier. https://doi.org/10.1016/B978-0-08-102065-4.00002-X.

Kregiel, D. (2014). Advances in biofilm control for food and beverage industry using organo-silane technology: A review. In *, 40. Food control* (pp. 32–40). Elsevier Ltd.. https://doi.org/10.1016/j.foodcont.2013.11.014. Issue 1.

Lee, W. C., Yusof, S., Hamid, N. S. A., & Baharin, B. S. (2006). Optimizing conditions for enzymatic clarification of banana juice using response surface methodology (RSM). *Journal of Food Engineering, 73*(1), 55–63. https://doi.org/10.1016/j.jfoodeng.2005.01.005

Liew Abdullah, A. G., Sulaiman, N. M., Aroua, M. K., Noor, M. M., & M. J.. (2007). Response surface optimization of conditions for clarification of carambola fruit juice using a commercial enzyme. *Journal of Food Engineering, 81*(1), 65–71. https://doi.org/10.1016/J.JFOODENG.2006.10.013

Lin, D., Ma, Y., Gu, J., Zou, L., Qin, W., & Wu, Z. (2024). Enhanced adsorption of deltamethrin by a SiO2 aerogel/chitosan/humic acid composite using co-precipitation method: Characterization and adsorption mechanism. *Industrial Crops and Products, 210*, Article 118137. https://doi.org/10.1016/J.INDCROP.2024.118137

Lu, Q., Li, Q., Zhang, J., Li, J., & Lu, J. (2016). Facile mesoporous template-assisted hydrothermal synthesis of ordered mesoporous magnesium silicate as an efficient adsorbent. *Applied Surface Science, 360*, 889–895. https://doi.org/10.1016/j.apsusc.2015.11.081

Mariod, A. A., & Fadul, H. (2013). Review: Gelatin, source, extraction and industrial applications. *Acta Scientiarum Polonorum. Technologia Alimentaria, 12*(2), 135–147.

Martín-Diana, A. B., Rico, D., Barat, J. M., & Barry-Ryan, C. (2009). Orange juices enriched with chitosan: Optimisation for extending the shelf-life. *Innovative Food Science and Emerging Technologies, 10*(4), 590–600. https://doi.org/10.1016/j.ifset.2009.05.003

Maximiano, P., Durães, L., & Simões, P. N. (2019). Organically-modified silica aerogels: A density functional theory study. *Journal of Supercritical Fluids, 147*, 138–148. https://doi.org/10.1016/j.supflu.2019.02.018

McKeown, I. P., & Nock, A. (1996). Improved beer stabilisation using silica gel. *Brauwelt International, 14*, 151–155.

Mierczynska-Vasilev, A., Boyer, P., Vasilev, K., & Smith, P. A. (2017). A novel technology for the rapid, selective, magnetic removal of pathogenesis-related proteins from wines. *Food Chemistry, 232*, 508–514. https://doi.org/10.1016/J.FOODCHEM.2017.04.050

Mirzaaghaei, M., Goli, S. A. H., & Fathi, M. (2016). Application of sepiolite in clarification of pomegranate juice: Changes on quality characteristics during process. *International Journal of Food Science and Technology, 51*(7), 1666–1673. https://doi.org/10.1111/ijfs.13138

Mohammadi, M., Rezaei Mokarram, R., Shahvalizadeh, R., Sarabandi, K., Lim, L. T., & Hamishehkar, H. (2020). Immobilization and stabilization of pectinase on an activated montmorillonite support and its application in pineapple juice clarification. *Food Bioscience, 36*. https://doi.org/10.1016/j.fbio.2020.100625

Mohseni-Bandpei, A., Eslami, A., Kazemian, H., Zarrabi, M., & Al-Musawi, T. J. (2020). A high density 3-aminopropyltriethoxysilane grafted pumice-derived silica aerogel as an efficient adsorbent for ibuprofen: Characterization and optimization of the adsorption data using response surface methodology. *Environmental Technology and Innovation, 18*. https://doi.org/10.1016/j.eti.2020.100642

Muley, A. B., Thorat, A. S., Singhal, R. S., & Harinath Babu, K. (2018). A tri-enzyme co-immobilized magnetic complex: Process details, kinetics, thermodynamics and applications. *International Journal of Biological Macromolecules, 118*, 1781–1795. https://doi.org/10.1016/J.IJBIOMAC.2018.07.022

Nayak, J. P., & Bera, J. (2009). *Preparation of Silica Aerogel by Ambient Pressure Drying Process using Rice Husk Ash as Raw Material. 68*. https://doi.org/10.1080/0371750X.2009.11082163. Issue 2.

Oliveira, R. J., De Conto, J. F., Oliveira, M. R., Egues, S. M. S., Borges, G. R., Dariva, C., & Franceschi, E. (2019). CO2/CH4 adsorption at high-pressure using silica-APTES aerogel as adsorbent and near infrared as a monitoring technique. *Journal of CO_2 Utilization, 32*, 232–240. https://doi.org/10.1016/j.jcou.2019.04.019

Orhan Dereli, B., Türkyılmaz, M., & Özkan, M. (2023). Clarification of pomegranate and strawberry juices: Effects of various clarification agents on turbidity, anthocyanins, colour, phenolics and antioxidant activity. *Food Chemistry, 413*. https://doi.org/10.1016/j.foodchem.2023.135672

Ouraipryvan, P., Sreethawong, T., & Chavadej, S. (2009). Synthesis of crystalline MgO nanoparticle with mesoporous-assembled structure via a surfactant-modified sol-gel process. *Materials Letters, 63*(21), 1862–1865. https://doi.org/10.1016/j.matlet.2009.05.068

Özkan, M. (2005). *Berrak Siyah Havuç Suyu Konsantresi Üretimi ve Antosiyaninlerin Isıl Stabilitesi*.

Özkan, M. (2014). *Kalecik Karası üzümlerden (Vitis vinifera L.) üretilen kırmızı üzüm suyunun çeşitli durultma yardımcı maddeleri ile durultulması ve durultmanın üzüm suyu rengi üzerine etkisi*.

Ozyilmaz, G., & Gunay, E. (2023). Clarification of apple, grape and pear juices by co-immobilized amylase, pectinase and cellulase. *Food Chemistry, 398*. https://doi.org/10.1016/j.foodchem.2022.133900

Parida, S. K., Dash, S., Patel, S., & Mishra, B. K. (2006). Adsorption of organic molecules on silica surface. *In advances in colloid and Interface science, 121*(1–3), 77–110. https://doi.org/10.1016/j.cis.2006.05.028

Patel, R. P., Purohit, N. S., & Suthar, A. M. (2009). An overview of silica aerogels. *In international Journal of ChemTech research CODEN, 1*(4).

Puškaš, V. S., & Miljić, U. D. (2012). Effects of fining on phenolic compounds and colour of red wine obtained with addition of increased amounts of grape solid phase in pomace. *Hemijska Industrija, 66*(5), 727–734. https://doi.org/10.2298/HEMIND111209018P

Qin, G., Yao, Y., Wei, W., & Zhang, T. (2013). Preparation of hydrophobic granular silica aerogels and adsorption of phenol from water. *Applied Surface Science, 280*, 806–811. https://doi.org/10.1016/j.apsusc.2013.05.066

Ramezani, M., Ferrentino, G., Morozova, K., Kamrul, S. M. H., & Scampicchio, M. (2020). Clarification of apple juices with vegetable proteins monitored by multiple light scattering. *Journal of Food Science, 85*(2), 316–323. https://doi.org/10.1111/1750-3841.14984

Ribéreau-Gayon, P., Glories, Y., Maujean, A., & Dubourdieu, D. (2006). *Handbook of enology volume 2 the chemistry of wine stabilization and treatments 2 nd edition*.

Rommel, A., Heatherbell, D. A., & Wrolstad, R. E. (1990). *Red raspberry juice and wine: Effect of processing and storage on anthocyanin pigment composition* (Color and Appearance).

Schulz, A., Woolley, R., Tabarin, T., & McDonagh, C. (2011). Dextran-coated silica nanoparticles for calcium-sensing. *Analyst, 136*(8), 1722–1727. https://doi.org/10.1039/c0an01009j

Siebert, K. J. (1999). Effects of protein-polyphenol interactions on beverage haze, stabilization, and analysis. In. *Journal of Agricultural and Food Chemistry, 47*(2), 353–362. https://doi.org/10.1021/jf980703o

Siebert, K. J., Carrasco, A., & Lynn, P. Y. (1996). *Formation of protein-polyphenol haze in beverages*.

Sojitra, U. V., Nadar, S. S., & Rathod, V. K. (2016). A magnetic tri-enzyme nanobiocatalyst for fruit juice clarification. *Food Chemistry, 213*, 296–305. https://doi.org/10.1016/j.foodchem.2016.06.074

Soleimani Dorcheh, A., & Abbasi, M. H. (2008). Silica aerogel; synthesis, properties and characterization. *In Journal of materials processing technology, 199*(1), 10–26. https://doi.org/10.1016/j.jmatprotec.2007.10.060

Soylu, T. M., Özel, C., Karakuzu Ikizler, B., Özarslan, A. C., Terzioğlu, P., Elalmis, Y. B., & Yücel, S. (2024). Mesoporous silica aerogels for sunflower oil refining and investigation of their adsorption performance. *Journal of Sol-Gel Science and Technology*. https://doi.org/10.1007/s10971-024-06395-9

Stankovic, S., Jovic, S., Zivkovic, J., & Pavlovic, R. (2012). Influence of age on red wine colour during fining with bentonite and gelatin. *International Journal of Food Properties, 15*(2), 326–335. https://doi.org/10.1080/10942912.2010.487625

Tastan, O., & Baysal, T. (2015). Clarification of pomegranate juice with chitosan: Changes on quality characteristics during storage. *Food Chemistry, 180*, 211–218. https://doi.org/10.1016/j.foodchem.2015.02.053

The European Food Safety Authority (EFSA). (2005). Opinion of the Scientific Panel on food additives, flavourings, processing aids and materials in contact with food (AFC) related to a 10th list of substances for food contact materials. *In EFSA Journal, 3*(10). https://doi.org/10.2903/j.efsa.2005.273a. Wiley-Blackwell Publishing Ltd.

Tiryaki, E., Başaran Elalmış, Y., Karakuzu İkizler, B., & Yücel, S. (2020). Novel organic/inorganic hybrid nanoparticles as enzyme-triggered drug delivery systems: Dextran and dextran aldehyde coated silica aerogels. *Journal of Drug Delivery Science and Technology, 56*. https://doi.org/10.1016/j.jddst.2020.101517

Turfan, Ö., Türkyilmaz, M., Yemi, O., & Özkan, M. (2011). Anthocyanin and colour changes during processing of pomegranate (Punica granatum L.; cv. Hicaznar) juice from sacs and whole fruit. *Food Chemistry, 129*(4), 1644–1651. https://doi.org/10.1016/j.foodchem.2011.06.024

Turfan, Ö., Türkyılmaz, M., Yemis, O., & Özkan, M. (2011). *Anthocyanin and colour changes during processing of pomegranate (Punica granatum L., cv. Hicaznar) juice from sacs and whole fruit.*. https://doi.org/10.1016/j.foodchem.2011.06.024

Türkyılmaz, M., Hamzaoğlu, F., & Özkan, M. (2020). Combined use of hydrocolloids in pomegranate juice and their effects on clarification and copigmentation. *International Journal of Food Science and Technology, 55*(4), 1426–1436. https://doi.org/10.1111/ijfs.14409

Türkyilmaz, M., & Özkan, M. (2014). Effects of condensed tannins on anthocyanins and colour of authentic pomegranate (Punica granatum L.) juices. *Food Chemistry, 164*, 324–331. https://doi.org/10.1016/J.FOODCHEM.2014.05.048

Türkyilmaz, M., Yemi, O., & Özkan, M. (2012). Clarification and pasteurisation effects on monomeric anthocyanins and percent polymeric colour of black carrot (Daucus carota L.) juice. *Food Chemistry, 134*(2), 1052–1058. https://doi.org/10.1016/J.FOODCHEM.2012.03.013

Ulker, Z., & Erkey, C. (2014). An emerging platform for drug delivery: Aerogel based systems. In *, 177*. *Journal of controlled release* (pp. 51–63). Elsevier B.V. https://doi.org/10.1016/j.jconrel.2013.12.033. Issue 1.

Van Sluyter, S. C., McRae, J. M., Falconer, R. J., Smith, P. A., Bacic, A., Waters, E. J., & Marangon, M. (2015). Wine protein haze: Mechanisms of formation and advances in prevention. *Journal of Agricultural and Food Chemistry, 63*(16), 4020–4030. https://doi.org/10.1021/ACS.JAFC.5B00047/ASSET/IMAGES/MEDIUM/JF-2015-00047W_0009.GIF

Wang, Y., & Ye, L. (2021). Haze in Beer: Its Formation and Alleviating Strategies, from a Protein–Polyphenol Complex Angle. *Foods, 10*(12). https://doi.org/10.3390/FOODS10123114

Waterhouse, A. L. (2002). Determination of Total Phenolics. *Current protocols in food. Analytical Chemistry, 6*(1). https://doi.org/10.1002/0471142913.FAI0101S06. I1.1.1-I1.1.8.

Wu, G., Liu, X., Wu, S., Zhou, J., Wang, Y., & Wu, C. (2024). Effect of metal ions on haze formation in blackberry wine. *LWT, 191*, Article 115628. https://doi.org/10.1016/j.lwt.2023.115628

Yilmaz, Y., & Toledo, R. T. (2004). Major Flavonoids in grape seeds and skins: Antioxidant capacity of Catechin, Epicatechin, and Gallic acid. *Journal of Agricultural and Food Chemistry, 52*(2), 255–260. https://doi.org/10.1021/jf030117h

Yücel, S., Karakuzu, B., Terzioğlu, P., & Temel, T. M. (2016). Influence of gel aging time on the properties of various silica aerogels synthesized from water glass. *Materials Science Forum, 866*, 176–180. https://doi.org/10.4028/www.scientific.net/MSF.866.176

Zhang, Y., Zhao, Q., Wang, H., Jiang, X., & Cha, R. (2017). Preparation of green and gelatin-free nanocrystalline cellulose capsules. *Carbohydrate Polymers, 164*, 358–363. https://doi.org/10.1016/J.CARBPOL.2017.01.096

Zhou, D. D., Li, J., Xiong, R. G., Saimaiti, A., Huang, S. Y., Wu, S. X., … Bin, H. (2022). Bioactive compounds, health benefits and food applications of grape. *In foods, 11*(18). https://doi.org/10.3390/foods11182755. MDPI.